Check for updates

Special Issue Article

Institution of MECHANICAL ENGINEERS
Journal of SYSTEMS AND CONTROL ENGINEERING

Proc IMechE Part I:
J Systems and Control Engineering
227(10) 752–763
© IMechE 2013
Reprints and permissions:
sagepub.co.uk/journalsPermissions.nav
DOI: 10.1177/0959651813500486
pii.sagepub.com
SAGE

On time-optimal trajectory planning for a flexible link robot

Klemens Springer, Hubert Gattringer and Peter Staufer

Abstract

This article focuses on time-optimal trajectory planning for robots with flexible links. Minimum time trajectories along specified paths as well as time-optimal point-to-point motions, which avoid vibration excitation due to elastic deflections, are determined. This is achieved by additionally constraining parts of the generalized forces and generalized force derivatives, resulting from the elastic potential. Therefore, the dynamical robot model is obtained using the Projection Equation. In a further step, a reduced model with the most essential degrees of freedom and sufficient accuracy is introduced, resulting in a flat system. Utilizing this, a trajectory control with an exact feedforward linearization in combination with a feedback part, consisting of a motor joint as well as a joint torque control, is realized. This nearly ideal control is used for moving on the time-optimal trajectories. The optimization is conducted with respect to velocity, jerk and motor torques as well as the newly introduced constraints, computable due to the flatness of the system. Experimental results demonstrate the improvement concerning vibration avoidance of the considered robot. Furthermore, a comparison between the occurring bending stress and the maximum permissible bending stress shows that mechanical damage is prevented with the use of the additional constraints.

Keywords

Dynamical modeling, flexible structures, optimal path-planning, nonlinear control, real-time systems

Date received: 2 April 2013; accepted: 12 July 2013

Introduction

A main trend in today's automation industry is the wish to construct lightweight robots to reduce process time and material costs for affordable production as well as to reduce energy consumption. Serious drawbacks of this development are inevitable structure elasticities that result in a bad control performance. Due to this fact, considerable research was done in the last decades concerning the control of such robotic manipulators.[1–3] Furthermore, path-constrained time-optimal motions (PCTOMs) as well as point-to-point time-optimal motions (PTPTOMs) may induce intense oscillations due to the elastic deformations of such a lightweight manipulator (called flexible link robot henceforth). As a consequence, lots of different techniques have been devised to address the problem of reducing elastic vibrations at the tool center point (TCP) when performing time-optimal trajectories. The easiest method to overcome this problem would be the use of advanced control algorithms,[4] but this turned out to be not as efficient with the given robot due to the highly elastic structure. Another method, which does not claim time-optimality, is to minimize the residual vibration excitation through utilizing a genetic optimization approach.[5] A more advanced technique, according to the authors Zhao and Chen,[6] tries to cope with this problem formulating a multistage optimization that minimizes the path duration in the first step and the control effort in the second step, which should lead to less structural excitation as well. This energy optimal objective used for vibrationless trajectories is at the expense of motion duration unfortunately. The simultaneous existence of bounds on both generalized forces (GFs) and generalized force derivatives (GFDs) was, to the authors' knowledge, first explicitly mentioned by Shin and McKay[7] and is also useful for time-optimal trajectories with less vibration excitation, but at the expense of motion duration as well. This article illustrates a novel technique to overcome the oscillations utilizing additional constraints, based on limiting-only parts of the GFs and GFDs that depend

Institute for Robotics, Johannes Kepler University Linz, Linz, Austria

Corresponding author:
Klemens Springer, Institute for Robotics, Johannes Kepler University Linz, Altenbergerstraße 69, 4040 Linz, Austria.
Email: klemens.springer@jku.at

on the elastic deflections in order to minimize motion duration. The limited term affects the vibration excitation of the flexible links and is the primary restriction in the resulting problem formulation. Similar to most of the methods for time-optimal path tracking that have been proposed in Pfeiffer et al.,[8] Shiller,[9] Constantinescu and Croft[10] and Verscheure et al.,[11] the one used here exploits that motion along a predefined path can be described by a single path coordinate σ. Time-optimal point-to-point motion optimization is done utilizing piecewise constant step functions. The calculation of these trajectories is, as it is already done for rigid robots in Gattringer et al.,[12] carried out with MUSCOD-II. This software package, developed by the Interdisciplinary Center for Scientific Computing at the University of Heidelberg, is utilized for computing the trajectories for a robot with three flexible links. For the verification of the expected improvements due to the proposed time-optimal problem formulation, experimental results concerning the acceleration at the TCP when performing the computed trajectories at the elastic robot built at the Institute for Robotics of the Johannes Kepler University Linz are presented.

This article is organized as follows: section "Setup" introduces the setup and section "Dynamics" the dynamical model of the used robot. The implemented control algorithm is discussed in section "Control." A verification of the system and the performance of the control design are shown in section "Model and control verification." In section "Optimization," the optimization of vibrationless PCTOMs as well as PTPTOMs is developed. Measurement results and a comparison to demonstrate the efficiency of this strategy are shown in section "Results."

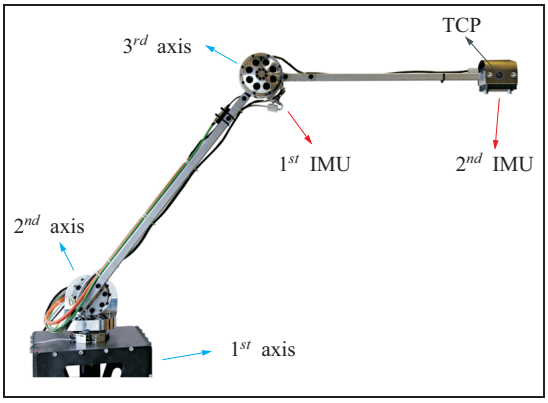

Figure 1. Setup of the elastic robot built at the Institute for Robotics at the Johannes Kepler University Linz.

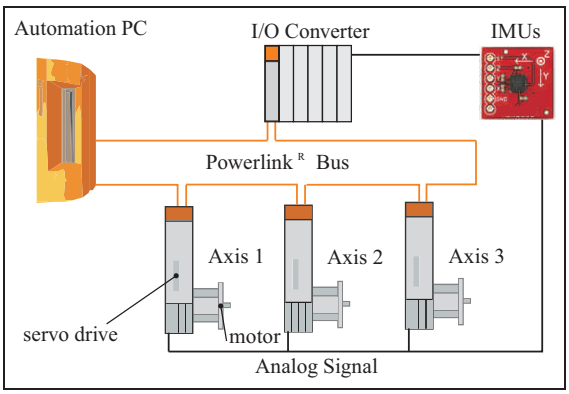

Figure 2. Electrical setup.
I/O: input/output; IMU: inertial measurement unit; PC: personal computer.

Setup

The mechanical setup under consideration, shown in Figure 1, has a maximum payload of 5 kg and square hollow cross-sections for both links, which have a length of about 1 m. The lightweight and elastic structure is driven by synchronous motors and *Harmonic Drive* gears for all three axes. Furthermore, the elasticities from the two flexible links as well as from the gears are taken into account. For improving the control performance, triple-axes analog angular rate and acceleration sensors, combined in an inertial measurement unit (IMU), are mounted at the third axis and at the TCP. Figure 2 shows the main components of the electrical setup. A central computing unit (Automation PC) with 400 μs cycle time communicates via an Ethernet Powerlink bus with the servo drives. Via this bus system, which is based on the Automation PCs cycle time, the IMUs are linked to the computing unit using input/output (I/O) converters (200–400 μs sampling time). With this configuration, a minimal time delay of 1.5–1.6 ms is achieved, resulting from a read operation from the IMU to a write command to the servo drives. This state-of-the-art realization allows very short cycle times. Nevertheless, this setup is too slow for a high-performance control task concerning vibration damping. Therefore, the IMUs are directly connected to the servo drives as well, leading to lower time delays and faster responses of the system. However, this requires that the entire feedback control is calculated on the servo drives to exploit this advantage.

Dynamics

The mathematical model of the considered system with N bodies is obtained with the Projection Equation described in detail in Bremer.[13] This method projects the linear and angular momenta, ${}_R\mathbf{p}_i = m_i {}_R\mathbf{v}_{c,i}$ and ${}_R\mathbf{L}_i = {}_R\mathbf{J}_i^c {}_R\boldsymbol{\omega}_{c,i}$, as well as the impressed forces and moments, ${}_R\mathbf{f}_i^e$ and ${}_R\mathbf{M}_i^e$, formulated in a body-fixed reference frame R (left subscript) in the direction of unconstrained motion. Therefore, the Jacobian matrices $(\partial_R \mathbf{v}_c / \partial \dot{\mathbf{q}})_i$ and $(\partial_R \boldsymbol{\omega}_c / \partial \dot{\mathbf{q}})_i$ using the minimal velocities $\dot{\mathbf{q}}$ are required. The advantage of the *Projection Equation* is the possibility of describing the linear and angular momenta of each body in separate reference frames.

For the sake of simplicity, a body-fixed reference frame R is used here. The variables ${}_R\mathbf{v}_{c,i}$ and ${}_R\boldsymbol{\omega}_{c,i}$ denote the linear and angular velocities of the center of gravity of the ith body. Mass and moments of inertia for each body i are represented by m_i and ${}_R\mathbf{J}_i^c$. In order to obtain a compact notation, the abbreviations

$$\begin{pmatrix} {}_R\mathbf{p} \\ {}_R\mathbf{L} \end{pmatrix}_i = \underbrace{\begin{bmatrix} m\mathbf{E} & 0 \\ 0 & {}_R\mathbf{J}^c \end{bmatrix}_i}_{\overline{\mathbf{M}}_i} \underbrace{\begin{pmatrix} {}_R\mathbf{v}_c \\ {}_R\boldsymbol{\omega}_c \end{pmatrix}_i}_{\dot{\mathbf{y}}_i} = \overline{\mathbf{M}}_i\dot{\mathbf{y}}_i \tag{1}$$

with $\dot{\mathbf{y}}_i$ denoting nonholonomic describing velocities for each body i, are introduced. Utilizing the Jacobian matrices, the projection in the direction of unconstrained motion of the linear and angular momenta of equation (1) and its time derivatives as well as the impressed forces yield the Projection Equation

$$\sum_{i=1}^{N} \underbrace{\begin{bmatrix} \left(\frac{\partial_R\mathbf{v}_c}{\partial\dot{\mathbf{q}}}\right)^T & \left(\frac{\partial_R\boldsymbol{\omega}_c}{\partial\dot{\mathbf{q}}}\right)^T \end{bmatrix}_i}_{\mathbf{F}_i^T} \underbrace{\begin{bmatrix} \left({}_R\dot{\mathbf{p}} + {}_R\tilde{\boldsymbol{\omega}}_{IR}\,{}_R\mathbf{p} - {}_R\mathbf{f}^e\right) \\ \left({}_R\dot{\mathbf{L}} + {}_R\tilde{\boldsymbol{\omega}}_{IR}\,{}_R\mathbf{L} - {}_R\mathbf{M}^e\right) \end{bmatrix}_i}_{\overline{\mathbf{M}}_i\ddot{\mathbf{y}}_i + \overline{\mathbf{G}}_i\dot{\mathbf{y}}_i - \overline{\mathbf{Q}}_i^e} = \mathbf{0} \tag{2}$$

There the matrices

$$\begin{aligned} \overline{\mathbf{G}}_i &= \begin{bmatrix} {}_R\tilde{\boldsymbol{\omega}}_{IR} & 0 \\ 0 & {}_R\tilde{\boldsymbol{\omega}}_{IR} \end{bmatrix}_i \overline{\mathbf{M}}_i \\ \overline{\mathbf{Q}}_i^e &= \begin{pmatrix} {}_R\mathbf{f}^e \\ {}_R\mathbf{M}^e \end{pmatrix}_i \end{aligned} \tag{3}$$

are used. The spin tensor ${}_R\tilde{\boldsymbol{\omega}}_{IR}$ describes the (absolute) angular velocity of the selected reference frame. Note that $\mathbf{y}_i$ itself does not appear in calculation anywhere. With the use of the describing velocities

$$\dot{\mathbf{y}}_i = \begin{pmatrix} {}_R\mathbf{v}_c \\ {}_R\boldsymbol{\omega}_c \end{pmatrix}_i = \begin{pmatrix} \left(\frac{\partial_R\mathbf{v}_c}{\partial\dot{\mathbf{q}}}\right) \\ \left(\frac{\partial_R\boldsymbol{\omega}_c}{\partial\dot{\mathbf{q}}}\right) \end{pmatrix}_i \dot{\mathbf{q}} = \mathbf{F}_i\dot{\mathbf{q}} \tag{4}$$

and accelerations

$$\ddot{\mathbf{y}}_i = \dot{\mathbf{F}}_i\dot{\mathbf{q}} + \mathbf{F}_i\ddot{\mathbf{q}} \tag{5}$$

of the ith body, the equations of motion for the system result out of equation (2) in minimal description

$$\mathbf{M}(\mathbf{q})\ddot{\mathbf{q}} + \mathbf{G}(\mathbf{q},\dot{\mathbf{q}})\dot{\mathbf{q}} - \mathbf{Q}(\mathbf{q},\dot{\mathbf{q}}) = 0 \tag{6}$$

The positive definite and symmetric mass matrix $\mathbf{M}$, the gyroscopic matrix $\mathbf{G}$, consisting of Coriolis and centrifugal terms and the vector of GFs $\mathbf{Q}$ in equation (6) are computed state dependent to

$$\begin{aligned} \mathbf{M}(\mathbf{q}) &= \sum_{i=1}^{N} \mathbf{F}_i^T\overline{\mathbf{M}}_i\mathbf{F}_i \\ \mathbf{G}(\mathbf{q},\dot{\mathbf{q}}) &= \sum_{i=1}^{N} \mathbf{F}_i^T\left(\overline{\mathbf{G}}_i\mathbf{F}_i + \overline{\mathbf{M}}_i\dot{\mathbf{F}}_i\right) \\ \mathbf{Q}(\mathbf{q},\dot{\mathbf{q}}) &= \sum_{i=1}^{N} \mathbf{F}_i^T\overline{\mathbf{Q}}_i^e \end{aligned} \tag{7}$$

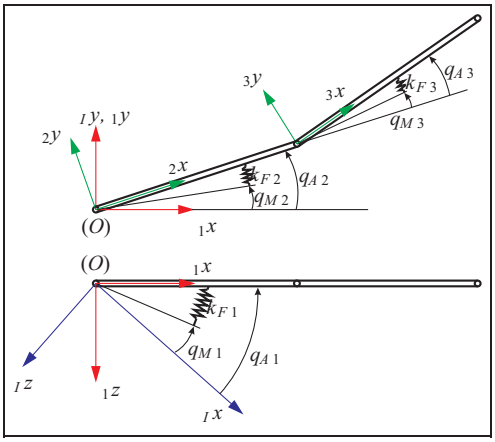

Figure 3. Illustration of the elastic deformations.

Control

In literature, several solutions to the trajectory tracking problem for elastic robots exist, such as inverse dynamics or fuzzy control. A two-degree-of-freedom control scheme is used here that consists of a feedforward and a feedback part. In order to build up a dynamical model for control purposes, it is reduced to the most essential degrees of freedom, which are characterized by the elasticities of the two flexible beams and driving units with large gear ratios. All elasticities are subsumed in one elasticity for each driving unit, represented with equivalent spring-damper systems. Hence, the equations of motion between the motor units and links are coupled only by the torque due to the elastic potential (bending moment)

$$\mathbf{Q}_A = \mathbf{K}(\mathbf{q}_M - \mathbf{q}_A) \tag{8}$$

with the stiffness matrix $\mathbf{K}$, $\mathbf{q}_M$ and $\mathbf{q}_A$ are representing the motor (subscript M) and link coordinates (subscript A), respectively. This leads to the set of minimal coordinates

$$\mathbf{q} = \begin{pmatrix} \mathbf{q}_M \\ \mathbf{q}_A \end{pmatrix} \tag{9}$$

that refers to a coordinate choice and gear potentials $V_{el,i} = k_{Fi}(\mathbf{q}_{Ai} - \mathbf{q}_{Mi})^2/2$ according to Figure 3.

In this context, the system of equation (2) is split into N_M differential equations for motor coordinates and a system of N_A link equations

$$\begin{aligned} \mathbf{Q}_A &= \sum_{i=1}^{N_A} \mathbf{F}_{A,i}^T\left[\overline{\mathbf{M}}_A\ddot{\mathbf{y}}_A + \overline{\mathbf{G}}_A\dot{\mathbf{y}}_A - \mathbf{Q}_A^e\right]_i \\ &= -\sum_{i=1}^{N_M} \mathbf{F}_{M,i}^T\left[\overline{\mathbf{M}}_M\ddot{\mathbf{y}}_M - \mathbf{Q}_M^e\right]_i \end{aligned} \tag{10}$$

where all gravity forces are included in $\mathbf{Q}_A^e$. In equation (10), the simplifying assumption is used that the angular velocity of the (motor) rotors is only due to their own spinning, that is

$$\boldsymbol{\omega}_{M,i} = \left(0, 0, \dot{q}_{M,i}\right)^T, \quad i = 1 \ldots 3 \tag{11}$$

for a rotation about the local z-axis.[14] As a consequence, the equations of motion for a robot with m axes of equation (10) are rewritten in combination with equations (4) and (5) to

$$\mathbf{Q}_M = \mathbf{M}_M \ddot{\mathbf{q}}_M + \mathbf{Q}_A + \mathbf{Q}_F \in \mathbb{R}^m \tag{12}$$

$$\mathbf{0} = \mathbf{M}_A \ddot{\mathbf{q}}_A + \mathbf{G}_A \dot{\mathbf{q}}_A - \mathbf{Q}_{G,A} - \mathbf{Q}_A \in \mathbb{R}^m \tag{13}$$

$$\mathbf{Q}_A = \mathbf{K}(\mathbf{q}_M - \mathbf{q}_A) \in \mathbb{R}^m \tag{14}$$

with a motor torque vector $\mathbf{Q}_M$, a friction vector $\mathbf{Q}_F$ and a vector, including gravitational terms $\mathbf{Q}_{G,A}$. All matrices are obtained using equation (7) representing the projection in minimal space.

Based on this simplified model, a two-degree-of-freedom trajectory control is developed. The feedforward part $\mathbf{u}_{FF}$ is given by an exact feedforward linearization with $\mathbf{q}_A$ as the flat output $\mathbf{z}$[15] for a robot consisting of m axes. For a flat parametrization of the system, equation (14) is inserted into equation (13) and solved for $\mathbf{q}_M$

$$\mathbf{q}_M(\mathbf{z}, \dot{\mathbf{z}}, \ddot{\mathbf{z}}) = \mathbf{K}^{-1}\left(\mathbf{M}_A(\mathbf{z})\ddot{\mathbf{z}} + \mathbf{G}_A(\mathbf{z}, \dot{\mathbf{z}})\dot{\mathbf{z}} - \mathbf{Q}_{G,A}(\mathbf{z}, \dot{\mathbf{z}})\right) + \mathbf{z} \in \mathbb{R}^m \tag{15}$$

Then equation (12) yields the input torques

$$\mathbf{Q}_M = \mathbf{Q}_M\left(\mathbf{z}, \dot{\mathbf{z}}, \ddot{\mathbf{z}}, \mathbf{z}^{(3)}, \mathbf{z}^{(4)}\right) \in \mathbb{R}^m \tag{16}$$

as a function of the flat output with the time derivatives $\dot{\mathbf{q}}_M$ and $\ddot{\mathbf{q}}_M$ from equation (15). Feedforward control is achieved by using desired values (subscript d) for the flat output $\mathbf{z} = \mathbf{z}_d = \mathbf{q}_{A,d}$ and its time derivatives in equation (15) and results out of equation (16) to $\mathbf{u}_{FF} = \mathbf{Q}_{M,d}(\mathbf{z}_d, \dot{\mathbf{z}}_d, \ddot{\mathbf{z}}_d, \mathbf{z}_d^{(3)}, \mathbf{z}_d^{(4)})$. Hence, it is important to guarantee four times differentiability of the desired trajectory. The feedback part is computed to

$$\mathbf{u}_{FB} = \underbrace{\mathbf{K}_{PM}\left(\mathbf{q}_{M,d} - \mathbf{q}_M\right) + \mathbf{K}_{DM}\left(\dot{\mathbf{q}}_{M,d} - \dot{\mathbf{q}}_M\right)}_{\text{motor joint control}} + \underbrace{\mathbf{K}_{PQ}\left(\mathbf{Q}_{A,d} - \mathbf{Q}_A\right) + \mathbf{K}_{DQ}\left(\dot{\mathbf{Q}}_{A,d} - \dot{\mathbf{Q}}_A\right)}_{\text{joint torque control}} \in \mathbb{R}^m \tag{17}$$

according to Siciliano and Khatib.[14] The first term represents the control of the motor joint position and the second term the control of the joint torque due to the elastic potential. Therefore, $\mathbf{Q}_{A,d}$ is calculated with equations (14) and (15) to

$$\mathbf{Q}_{A,d} = \mathbf{K}(\mathbf{q}_M(\mathbf{z}_d, \dot{\mathbf{z}}_d, \ddot{\mathbf{z}}_d) - \mathbf{z}_d) \tag{18}$$

Because of the fact that no measurement of $\mathbf{Q}_A$ is available, an appropriate estimation is obtained according to Staufer and Gattringer[16] by reconstructing the link dynamics using the Projection Equation (2)

$$\mathbf{Q}_A \approx \sum_{i=2}^{3} \left(\frac{\partial_i \mathbf{v}}{\partial \dot{\mathbf{q}}_A}\right)_i^T \left[m({}_i\dot{\mathbf{v}} + {}_i\tilde{\boldsymbol{\omega}}_{Ii}\, {}_i\mathbf{v} - {}_i\mathbf{g})\right]_i \tag{19}$$

Thereby, lumped masses are assumed at the third axis (mass m_2 and length l_2) and on the tip body (mass m_3 and length l_3), and the inertia parameters are ignored (the inertia of link 1 is included in the motor of the base). Neglecting the effects of inertia is permissible due to the dominating Steiner term in the considered system. Using acceleration sensors mounted at the third axis and the TCP, see Figure 1, the torque is approximately calculated to

$$\mathbf{Q}_A \approx m_2 \left(\frac{\partial_2 \mathbf{v}_2}{\partial \dot{\mathbf{q}}_A}\right)^T {}_2\mathbf{a}_1 + m_3 \left(\frac{\partial_3 \mathbf{v}_3}{\partial \dot{\mathbf{q}}_A}\right)^T {}_3\mathbf{a}_2 \tag{20}$$

as a function of the accelerations and the link positions. The Jacobian matrices $(\partial_i \mathbf{v}/\partial \dot{\mathbf{q}}_A)_i$ depend on the link positions $\mathbf{q}_A$ and are therefore not known. Since $\mathbf{q}_M$ is close to $\mathbf{q}_A$ and the acceleration sensor signals dominate the result of $\mathbf{Q}_A$, it is sufficient to use the motor positions instead of $\mathbf{q}_A$ for the calculation of the Jacobians. The controller gains $\mathbf{K}_j \in \mathbb{R}^{m,m}, j = PM, DM, PQ, DQ$ in equation (17) are chosen as diagonal matrices. The two-degree-of-freedom trajectory control design is shown in Figure 4.

Model and control verification

A very important requirement for planning time-optimal trajectories, as well as for path-planning itself, is an appropriate kinematical as well as dynamical model. In order to show the sufficient correlation between the simulation model (sim) and the real robot (real), verification results concerning the accelerations at the TCP ${}_3\mathbf{a}_2 = [a_{x,2}, a_{y,2}, a_{z,2}]^T$ using conventional proportional–derivative (PD) control are presented in Figure 5. Due to the high accordance, the simplified model can be considered as adequate.

For the verification of the proposed control strategy, the implementation of the control structure in Figure 4 is explained briefly. The motor angles $\mathbf{q}_M$ and angular rates $\dot{\mathbf{q}}_M$ are given by the resolvers. The torque due to the elastic potential $\mathbf{Q}_A$ as well as its derivative $\dot{\mathbf{Q}}_A$ are calculated by utilizing the acceleration signals ${}_2\mathbf{a}_1$ and ${}_3\mathbf{a}_2$, measured by the IMUs, see section "Control." The "trajectory generation" provides the path $\mathbf{z}_d$ with a discretization of $400\,\mu s$ through interpolating from $\bar{\mathbf{z}}_d = (\mathbf{q}_{A,d}, \dot{\mathbf{q}}_{A,d}, \ddot{\mathbf{q}}_{A,d}, \mathbf{q}_{A,d}^{(3)}, \mathbf{q}_{A,d}^{(4)})^T$, resulting from an optimization. Figure 6 compares the performance of a simple PD motor joint controller without a feedforward control (PD) with the flatness-based feedforward $\mathbf{u}_{FF}$ in combination with the feedback control from equation (17) using acceleration sensors (acceleration control (AC)). The plot shows the accelerations at the TCP ${}_3\mathbf{a}_2$, while tracking a straight line with a five times continuous trajectory, having the following performance specifications of the path of the TCP: length approximately 2.1 m, duration 1.05 s and maximum acceleration

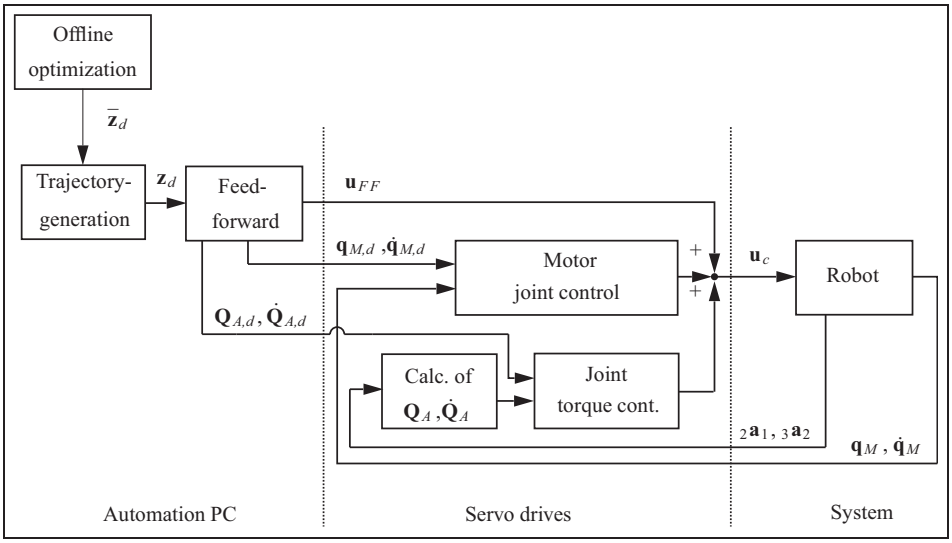

Figure 4. Control structure used for controlling the system when applying the optimized trajectories.

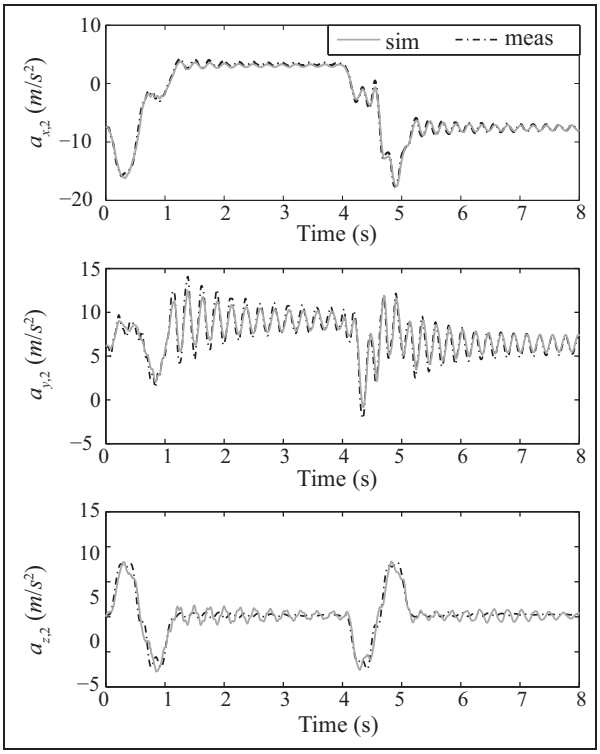

Figure 5. Verification of simulation (sim) and measured results (meas).

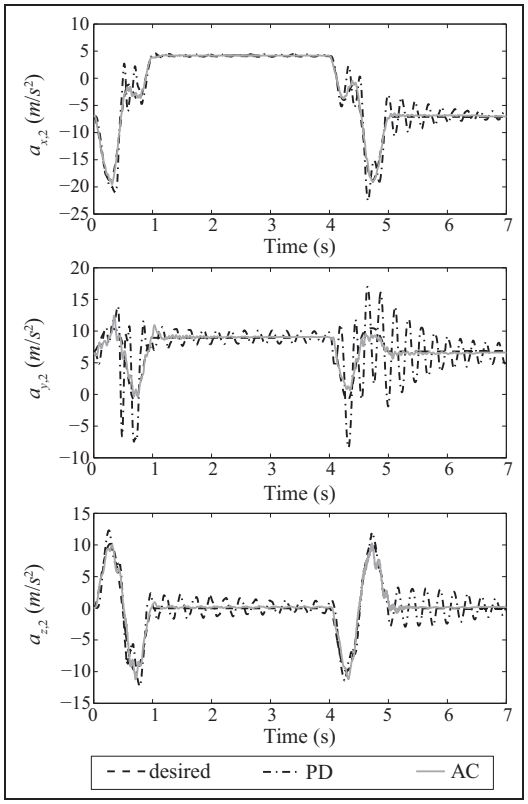

Figure 6. Verification of the used control design.
PD: proportional–derivative; AC: acceleration control.

$18\,\mathrm{m/s^2}$. Due to the minimal acceleration error, the assumption of a sufficient control is made.

Optimization

Before the main optimization problems, dealing with PCTOM and PTPTOM, are presented, the toolkit used for the optimization procedure, is introduced.

MUSCOD-II toolkit

MUSCOD-II gives the opportunity to solve differential algebraic equations (DAEs) in the form

$$B(t,\mathbf{x}(t),\mathbf{s}(t),\mathbf{u}_M(t),\eta)\frac{d}{dt}\mathbf{x}(t) = f(t,\mathbf{x}(t),\mathbf{s}(t),\mathbf{u}_M(t),\eta)$$
$$0 = g(t,\mathbf{x}(t),\mathbf{s}(t),\mathbf{u}_M(t),\eta) \quad (21)$$

with the matrix function B. The system state is described by the differential and algebraic state vectors $\mathbf{x}(t)$ and $\mathbf{s}(t)$. The system behavior is controlled by the control vector $\mathbf{u}_M(t)$ and the global design parameter vector $\boldsymbol{\eta}$. The objective function J is of generalized Bolza type, containing Lagrange and Mayer terms

$$J = \Phi(t_e, \mathbf{x}(t_e), \mathbf{s}(t_e), \boldsymbol{\eta}) + \int_0^{t_e} L(t, \mathbf{x}(t), \mathbf{s}(t), \boldsymbol{\eta}) dt \quad (22)$$

The original continuous problem is reformulated as a nonlinear programming problem (NLP), approximating the control functions by a piecewise representation on a finite number of subintervals, called multiple shooting intervals. In the direct multiple shooting method, the DAE is solved independently on each subinterval. This is done by an iterative solution procedure, a specially tailored sequential quadratic programming (SQP) algorithm. A far more complete description of the methods employed is given in Leineweber.[17]

Consideration of elastic terms

When planning a trajectory using an exact model of the system, in general, no vibration should occur at the TCP of the robot. Although a very good model was developed in section "Dynamics," small model uncertainties and parameter inaccuracies have to be assumed, and the control has to cope with the emerging tracking errors. In the case of a flexible link robot moving on time-optimal trajectories, this can lead to vibrations at the TCP. An idea to minimize these deflections for preventing mechanical damage and enabling sufficient control of the induced oscillation is to constrain the GFs resulting from the elastic potential of the robot. In order to understand the influence of the elastic structure of the robot during trajectory tracking, we reconsider the GFs due to the elastic potential

$$\begin{aligned}\mathbf{Q}_A &= \left(\frac{\partial \mathbf{V}_{el}}{\partial \mathbf{q}}\right)^T = \left(\frac{\partial}{\partial \mathbf{q}}\left(\sum_{i=1}^{3} \frac{1}{2} k_{Fi}(q_{Ai} - q_{Mi})^2\right)\right)^T \\ &= \mathbf{K}(\mathbf{q}_M - \mathbf{q}_A) \in \mathbb{R}^m\end{aligned} \quad (23)$$

Besides constraining the required physical limitations concerning the actuator torques $\mathbf{Q}_M$, motor angular rates $\dot{\mathbf{q}}_M$ and the jerk of the link angles $\mathbf{q}_A^{(3)}$, it is useful to include boundaries for expression (23). This will lead to slower motion on the one hand, but induces much less vibration at the TCP, on the other hand. Similarly, the GFDs are physically bounded as well. In the case of electric actuators, for example, the available supply voltage necessarily limits the GFs variation rate. But limiting the GFDs as a whole would lead to slow motion behavior. Hence, only the terms concerning the elastic potential resulting from equation (23) are considered, and therefore, $(d/dt)\mathbf{Q}_A$ is constrained as well. These types of constraints are additionally applied to a PCTOM and PTPTOM optimization, which is solved with MUSCOD-II introduced in section "MUSCOD-II toolkit."

PCTOM

A path $\mathbf{r}(\sigma) = [\,x(\sigma) \quad y(\sigma) \quad z(\sigma)\,]^T$, given in task space coordinates x, y and z, is considered as a function of a scalar path coordinate $\sigma \in [0, 1]$. It determines the spatial geometry of the path, whereas the trajectory's time dependency follows from the relation $\sigma(t)$ between the path coordinate σ and time t. For the given path, the velocities, accelerations, jerks and fourth derivatives can be rewritten as

$$\begin{aligned}\dot{\mathbf{r}}(\sigma, \dot{\sigma}) &= \mathbf{r}'(\sigma)\dot{\sigma} \\ \ddot{\mathbf{r}}(\sigma, \dot{\sigma}, \ddot{\sigma}) &= \mathbf{r}'(\sigma)\ddot{\sigma} + \mathbf{r}''(\sigma)\dot{\sigma}^2 \\ \mathbf{r}^{(3)}\left(\sigma, \dot{\sigma}, \ddot{\sigma}, \sigma^{(3)}\right) &= \mathbf{r}'(\sigma)\sigma^{(3)} + 3\mathbf{r}''(\sigma)\dot{\sigma}\ddot{\sigma} + \mathbf{r}'''(\sigma)\dot{\sigma}^3 \\ \mathbf{r}^{(4)}\left(\sigma, \dot{\sigma}, \ddot{\sigma}, \sigma^{(3)}, \sigma^{(4)}\right) &= \mathbf{r}'(\sigma)\sigma^{(4)} \\ &\quad + \mathbf{r}''(\sigma)\left(4\dot{\sigma}\sigma^{(3)} + 3\ddot{\sigma}^2\right) + 6\mathbf{r}'''(\sigma)\dot{\sigma}^2\ddot{\sigma} + \mathbf{r}''''(\sigma)\dot{\sigma}^4\end{aligned} \quad (24)$$

The analytical inverse kinematics is used to determine the link coordinates $\mathbf{q}_A(\mathbf{r}(\sigma))$ and its derivatives $\dot{\mathbf{q}}_A$, $\ddot{\mathbf{q}}_A$, $\mathbf{q}_A^{(3)}$ and $\mathbf{q}_A^{(4)}$. These are required up to the fourth derivative due to the combination with the motor coordinates that are calculated to

$$\begin{aligned}\mathbf{q}_M &= \mathbf{q}_M(\mathbf{q}_A, \dot{\mathbf{q}}_A, \ddot{\mathbf{q}}_A) \\ \dot{\mathbf{q}}_M &= \dot{\mathbf{q}}_M\left(\mathbf{q}_A, \dot{\mathbf{q}}_A, \ddot{\mathbf{q}}_A, \mathbf{q}_A^{(3)}\right) \\ \ddot{\mathbf{q}}_M &= \ddot{\mathbf{q}}_M\left(\mathbf{q}_A, \dot{\mathbf{q}}_A, \ddot{\mathbf{q}}_A, \mathbf{q}_A^{(3)}, \mathbf{q}_A^{(4)}\right)\end{aligned} \quad (25)$$

see equation (15). Consequently, the minimal coordinates are written as a function of the path coordinate and its derivatives

$$\mathbf{q} = \begin{pmatrix}\mathbf{q}_M \\ \mathbf{q}_A\end{pmatrix} = \begin{pmatrix}\mathbf{q}_M(\sigma, \dot{\sigma}, \ddot{\sigma}) \\ \mathbf{q}_A(\sigma)\end{pmatrix} = \mathbf{q}(\sigma, \dot{\sigma}, \ddot{\sigma}) \quad (26)$$

Substituting expression (26) in the system dynamics (6), it is reformulated in dependence of the scalar path coordinate σ and its derivatives to compute the drive torques

$$\mathbf{Q}_M = \mathbf{M}(\mathbf{q}(\bar{\boldsymbol{\sigma}}))\ddot{\mathbf{q}}(\bar{\boldsymbol{\sigma}}, u) + \mathbf{g}(\mathbf{q}(\bar{\boldsymbol{\sigma}}), \dot{\mathbf{q}}(\bar{\boldsymbol{\sigma}})) - \mathbf{Q}_{res}(\bar{\boldsymbol{\sigma}}) \quad (27)$$

using the state vector $\bar{\boldsymbol{\sigma}} = [\,\sigma \quad \dot{\sigma} \quad \ddot{\sigma} \quad \sigma^{(3)}\,]^T$ and the input variable $u = \sigma^{(4)}$ (MUSCOD-II control variable $\mathbf{u}_M = u$). An integrator chain to calculate the path coordinate σ and its derivatives is given by

$$\underbrace{\dot{\bar{\boldsymbol{\sigma}}} = \frac{d}{dt}\begin{pmatrix}\sigma \\ \dot{\sigma} \\ \ddot{\sigma} \\ \sigma^{(3)}\end{pmatrix}}_{\dot{\bar{\boldsymbol{\sigma}}}} = \underbrace{\begin{pmatrix}0 & 1 & 0 & 0 \\ 0 & 0 & 1 & 0 \\ 0 & 0 & 0 & 1 \\ 0 & 0 & 0 & 0\end{pmatrix}\bar{\boldsymbol{\sigma}} + \begin{pmatrix}0 \\ 0 \\ 0 \\ 1\end{pmatrix} u}_{f(\bar{\boldsymbol{\sigma}}, u)} \quad (28)$$

In order to determine a time-optimal trajectory on a path, the optimization formulation can be given as

$$
\begin{aligned}
\min_{u} J(u) &= \int_0^{t_e} 1 dt \\
\text{s.t. } \dot{\bar{\boldsymbol{\sigma}}} &= f(\bar{\boldsymbol{\sigma}}, u) \\
\dot{\mathbf{q}}_{M,lb} &\leqslant \dot{\mathbf{q}}_M(\bar{\boldsymbol{\sigma}}, u) \leqslant \dot{\mathbf{q}}_{M,ub} \\
\mathbf{q}^{(3)}_{A,lb} &\leqslant \mathbf{q}^{(3)}_A(\bar{\boldsymbol{\sigma}}, u) \leqslant \mathbf{q}^{(3)}_{A,ub} \\
\mathbf{Q}_{M,lb} &\leqslant \mathbf{Q}_M(\bar{\boldsymbol{\sigma}}, u) \leqslant \mathbf{Q}_{M,ub} \\
\mathbf{Q}_{A,lb} &\leqslant \mathbf{Q}_A(\bar{\boldsymbol{\sigma}}, u) \leqslant \mathbf{Q}_{A,ub} \\
\dot{\mathbf{Q}}_{A,lb} &\leqslant \dot{\mathbf{Q}}_A(\bar{\boldsymbol{\sigma}}, u) \leqslant \dot{\mathbf{Q}}_{A,ub} \\
\sigma(0) &= 0, \sigma(t_e) = 1 \\
\dot{\sigma}(0) &= 0, \dot{\sigma}(t_e) = 0 \\
\dot{\sigma} &\geqslant 0 \\
&\text{for } t \in [0, t_e]
\end{aligned} \tag{29}
$$

with the lower and upper bounds $\mathbf{Q}_{M,lb}$ and $\mathbf{Q}_{M,ub}$, $\mathbf{Q}_{A,lb}$ and $\mathbf{Q}_{A,ub}$, $\dot{\mathbf{Q}}_{A,lb}$ and $\dot{\mathbf{Q}}_{A,ub}$, $\dot{\mathbf{q}}_{M,lb}$ and $\dot{\mathbf{q}}_{M,ub}$ and $\mathbf{q}^{(3)}_{A,lb}$ and $\mathbf{q}^{(3)}_{A,ub}$. From the solution of the optimization with MUSCOD-II and in combination with equations (28) and (24) and the inverse kinematics, the desired trajectory $\mathbf{q}_{A,d}(\sigma(t))$ and its derivatives are obtained.

PTPTOM

When calculating PTPTOM, the problem formulation has to be redefined. There are many ways to determine such trajectories. The procedure used here is to utilize piecewise constant functions for the fourth derivatives of the actuator coordinates $\mathbf{q}^{(4)}_A(t)$ along the unknown trajectory. An integrator chain to calculate the link coordinates $\mathbf{q}_A(t)$ is given by

$$
\dot{\mathbf{x}} = \frac{d}{dt}\begin{pmatrix} \mathbf{q}_A \\ \dot{\mathbf{q}}_A \\ \ddot{\mathbf{q}}_A \\ \mathbf{q}^{(3)}_A \end{pmatrix} = \underbrace{\begin{pmatrix} \mathbf{0} & \mathbf{E} & \mathbf{0} & \mathbf{0} \\ \mathbf{0} & \mathbf{0} & \mathbf{E} & \mathbf{0} \\ \mathbf{0} & \mathbf{0} & \mathbf{0} & \mathbf{E} \\ \mathbf{0} & \mathbf{0} & \mathbf{0} & \mathbf{0} \end{pmatrix}\begin{pmatrix} \mathbf{q}_A \\ \dot{\mathbf{q}}_A \\ \ddot{\mathbf{q}}_A \\ \mathbf{q}^{(3)}_A \end{pmatrix} + \begin{pmatrix} \mathbf{0} \\ \mathbf{0} \\ \mathbf{0} \\ \mathbf{E} \end{pmatrix}\mathbf{u}}_{f(\mathbf{x},\mathbf{u})} \tag{30}
$$

with the input variable $\mathbf{u} = \mathbf{q}^{(4)}_A$ (MUSCOD-II control vector $\mathbf{u}_M = \mathbf{u}$). The optimization formulation to determine a PTPTOM can be given

$$
\begin{aligned}
\min_{\mathbf{u}} J(\mathbf{u}) &= \int_0^{t_e} 1 dt \\
\text{s.t.} \quad \dot{\mathbf{x}} &= f(\mathbf{x}, \mathbf{u}) \\
\dot{\mathbf{q}}_{M,lb} &\leqslant \dot{\mathbf{q}}_M(\mathbf{x}, \mathbf{u}) \leqslant \dot{\mathbf{q}}_{M,ub} \\
\mathbf{q}^{(3)}_{A,lb} &\leqslant \mathbf{q}^{(3)}_A(\mathbf{x}, \mathbf{u}) \leqslant \mathbf{q}^{(3)}_{A,ub} \\
\mathbf{Q}_{M,lb} &\leqslant \mathbf{Q}_M(\mathbf{x}, \mathbf{u}) \leqslant \mathbf{Q}_{M,ub} \\
\mathbf{Q}_{A,lb} &\leqslant \mathbf{Q}_A(\mathbf{x}, \mathbf{u}) \leqslant \mathbf{Q}_{A,ub} \\
\dot{\mathbf{Q}}_{A,lb} &\leqslant \dot{\mathbf{Q}}_A(\mathbf{x}, \mathbf{u}) \leqslant \dot{\mathbf{Q}}_{A,ub} \\
\mathbf{q}(0) &= \mathbf{q}_0, \mathbf{q}(t_e) = \mathbf{q}_{end} \\
\dot{\mathbf{q}}(0) &= 0, \dot{\mathbf{q}}(t_e) = 0 \\
&\text{for } t \in [0, t_e]
\end{aligned} \tag{31}
$$

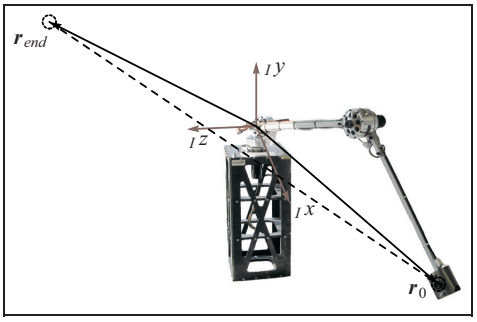

Figure 7. Straight line trajectory in space.

with the same lower and upper bounds as in section "PCTOM." The trajectory $\mathbf{q}_{A,d}(t)$ and its derivatives are computed as a result of the optimization again.

Results

This section draws a comparison between the experimental results with and without the consideration of the additional constraints of the terms $\mathbf{Q}_A$ and $\dot{\mathbf{Q}}_A$, introduced in section "Consideration of elastic terms." The trajectory for the path-constrained motion optimization is a straight line in space with the length of 2.1 m described through

$$
\mathbf{r}(\sigma) = \begin{pmatrix} x_0 + (x_{end} - x_0)\sigma \\ y_0 + (y_{end} - y_0)\sigma \\ z_0 + (z_{end} - z_0)\sigma \end{pmatrix}, \quad \sigma \in [0, 1] \tag{32}
$$

with $x_0 = 1.4\,\text{m}$, $x_{end} = 1.4\,\text{m}$, $y_0 = -0.5\,\text{m}$, $y_{end} = 1.0\,\text{m}$, $z_0 = -0.75\,\text{m}$ and $z_{end} = 0.75\,\text{m}$. This trajectory is shown in Figure 7.

For the point-to-point motion, the start and stop points required for the optimization in expression (31) are $\mathbf{q}_0(\mathbf{r}_0)$ and $\mathbf{q}_{end}(\mathbf{r}_{end})$ with

$$
\mathbf{r}_0 = \begin{pmatrix} x_0 \\ y_0 \\ z_0 \end{pmatrix}, \mathbf{r}_{end} = \begin{pmatrix} x_{end} \\ y_{end} \\ z_{end} \end{pmatrix} \tag{33}
$$

and the same values as for the path-constrained motion. The trajectories obtained by the optimization in sections "PCTOM" and "PTPTOM" are used for path generation and as a consequence as input for the control design, see Figure 4. The constraints are taken as $-\mathbf{Q}_{M,lb} = \mathbf{Q}_{M,ub} = 2.8\,\text{Nm}$, $-\mathbf{Q}_{A,lb} = \mathbf{Q}_{A,ub} = 185\,\text{Nm}$, $-\dot{\mathbf{Q}}_{A,lb} = \dot{\mathbf{Q}}_{A,ub} = 1200\,\text{Nm}/s$, $-\dot{\mathbf{q}}_{M,lb} = \dot{\mathbf{q}}_{M,ub} = [8.9, 8.9, 5.56]^T\,\text{rad/s}$ and $-\mathbf{q}^{(3)}_{A,lb} = \mathbf{q}^{(3)}_{A,ub} = [300, 360, 780]^T\,\text{rad/s}^3$.

For the PTPTOM, a minimum time of 0.648 s results. In contrast to the PCTOM case with a minimum time of 0.797 s, the improvement is about ≈18.7%. Figures 8 and 9 as well as Figures 10 and 11 illustrate that the accelerations at the third joint ${}_2\mathbf{a}_1 = [a_x, a_y, a_z]^T$ and at the TCP ${}_3\mathbf{a}_2 = [a_{x,2}, a_{y,2}, a_{z,2}]^T$ show much higher vibrational behavior without the additional constraints in both trajectory optimizations.

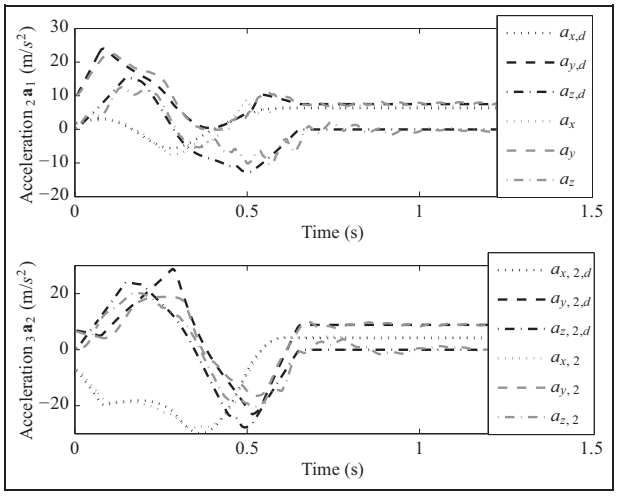

Figure 8. Accelerations at the third joint $_2\mathbf{a}_1$ and at the TCP $_3\mathbf{a}_2$ compared to the desired ones when applying the PTPTOM with additional constraints.

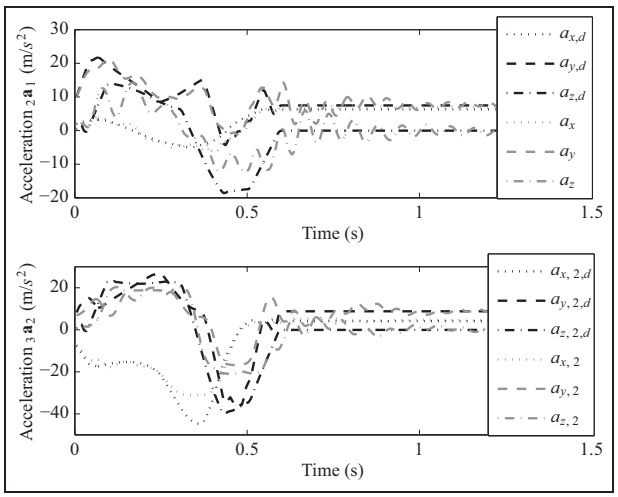

Figure 9. Accelerations at the third joint $_2\mathbf{a}_1$ and at the TCP $_3\mathbf{a}_2$ compared to the desired ones when applying the PTPTOM without additional constraints.

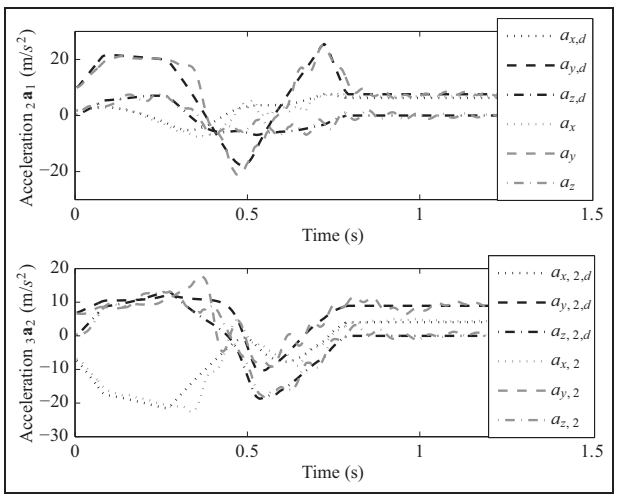

Figure 10. Accelerations at the third joint $_2\mathbf{a}_1$ and at the TCP $_3\mathbf{a}_2$ compared to the desired ones when applying the PCTOM with additional constraints.

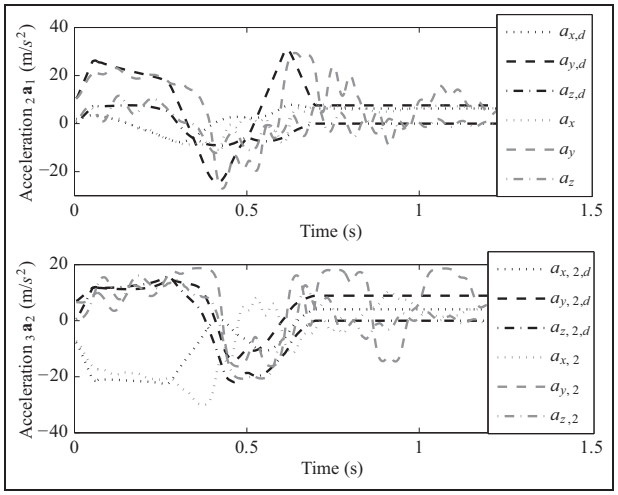

Figure 11. Accelerations at the third joint $_2\mathbf{a}_1$ and at the TCP $_3\mathbf{a}_2$ compared to the desired ones when applying the PCTOM without additional constraints.

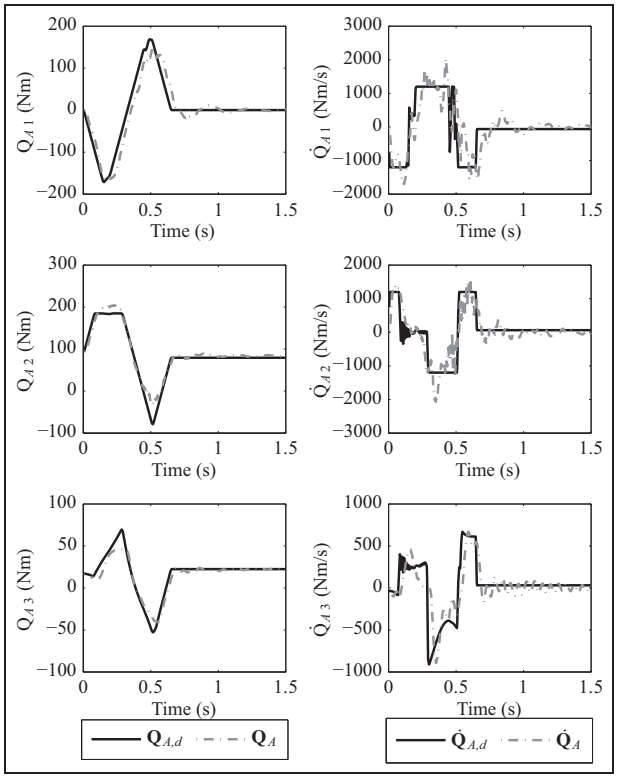

Figure 12. $\mathbf{Q}_A$ and $\dot{\mathbf{Q}}_A$ when applying the PTPTOM with additional constraints.

This can be seen in the PCTOM case in Figure 11 particularly, because of the fact that the track has to be slowed down proportionally in order to prevent mechanical damage in the PTPTOM case without additional constraints in Figure 9. Figure 12 shows that the desired additional constraints $\mathbf{Q}_{A,d} = [Q_{A1,d}, Q_{A2,d}, Q_{A3,d}]^T$, $\dot{\mathbf{Q}}_{A,d} = [\dot{Q}_{A1,d}, \dot{Q}_{A2,d}, \dot{Q}_{A3,d}]^T$ are satisfied very well in comparison to $\mathbf{Q}_A, \dot{\mathbf{Q}}_A$ obtained through the calculation using the acceleration signals of the IMUs. In contrast to that, Figure 13 illustrates

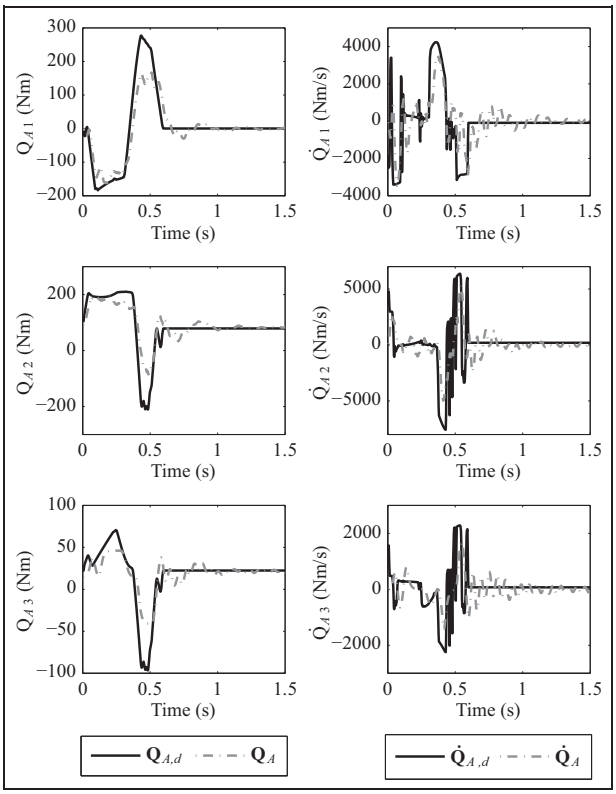

Figure 13. $\mathbf{Q}_A$ and $\dot{\mathbf{Q}}_A$ when applying the PTPTOM without additional constraints.

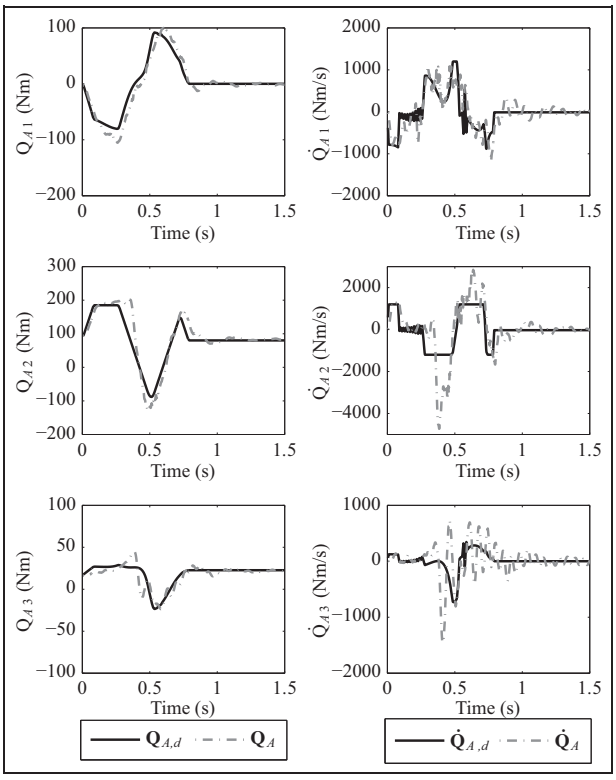

Figure 14. $\mathbf{Q}_A$ and $\dot{\mathbf{Q}}_A$ when applying the PCTOM with additional constraints.

that these terms are a lot higher without the additional constraints being active. The same effect results from the PCTOM case, shown in Figures 14 and 15. In summary, it can be said that the vibration excitation is nearly completely suppressed, when the parts of the GFs $\mathbf{Q}_A$ and its derivatives resulting from the elastic potential are constrained. This seems reasonable since a bound for $\mathbf{Q}_A$ equals a maximum permissible bending moment of the beam, and hence, less oscillations are induced.

Bending stress

When considering highly dynamical movements with flexible structures, one should keep in mind the occurring bending stress σ_b. This has to be compared to the maximum allowed bending stress σ_{max}, defined by given material parameters. Based on the simplified model from section "Control," the occurring bending stress computes to

$$\sigma_{b,i} = \frac{Q_{Ai}}{W_i}, \quad i = 1 \ldots 3 \tag{34}$$

with the bending moment $Q_{Ai}, \quad i = 1 \ldots 3$ (equals the GFs due to the elastic potential here). The section modulus W_i is required for two bending directions for the first beam as well as for one bending direction for the second beam. They are calculated with the information of having square hollow cross sections. The maximum permissible bending stress

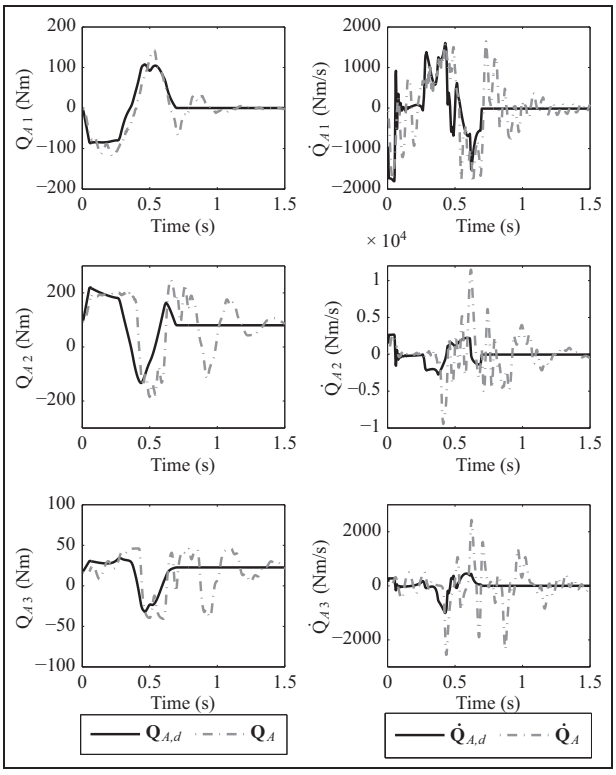

Figure 15. $\mathbf{Q}_A$ and $\dot{\mathbf{Q}}_A$ when applying the PCTOM without additional constraints.

$$\sigma_{max} = \frac{\sigma_{bS}}{SF} \tag{35}$$

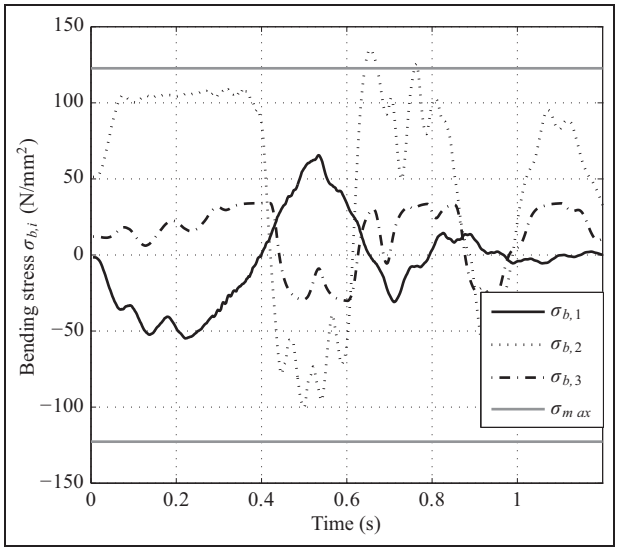

Figure 16. Bending stresses occurring for the PCTOM without additional constraints.

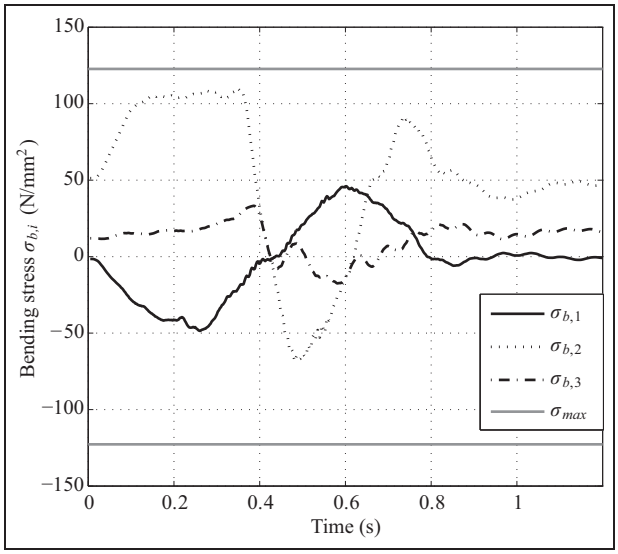

Figure 17. Bending stresses occurring for the PCTOM with additional constraints.

is calculated using the maximum bending stress $\sigma_{bS} = 270\,\mathrm{N/mm^2}$ for *S235* steel concerning dynamical swelling strains and a safety factor $SF = 2.2$. In Figure 16, one can see clearly on the basis of the PCTOM optimization, without additional constraints, that the bending stresses $\sigma_{b,1}, \sigma_{b,2}$ and $\sigma_{b,3}$ exceed the maximum permissible stress σ_{max}. In contrast to that, Figure 17 shows that σ_{max} is satisfied when optimizing with additional constraints. For further investigations, a comparison between the computation of the bending stresses with the use of acceleration sensors and the calculation using strain gauges would be interesting.

Discussion

Concerning the simplifications required for obtaining the reduced model, we have to keep in mind that the introduced dynamical model is used mainly for control and trajectory optimization, wherefore a trade-off between computational cost and model accordance is sufficient. An important advantage of this lumped element model is the possibility to derive a simple description of the flat outputs of the system, what is required for lots of different control concepts as well as the one used here. In summary, the introduced dynamical system can be considered as adequate for the used control and path-planning strategies.

With respect to control, one may note why not using standard concepts like, for example, I/O linearization for controlling the given robotic system. These and also passive vibration damping methods that do a correction of the desired trajectory, for example, as proposed in Bremer,[13] do not yield sufficient oscillation avoidance. This is substantiated by the fact that even small parameter uncertainties can lead to intense structural vibrations. Thus, additional active vibration damping is necessary and fulfilled with the proposed approach. Thereby, acceleration sensors are used for the calculation of the torque $\mathbf{Q}_A$ due to the much easier mounting in contrast to strain gauges. As the verification in section "Model and control verification" has shown, the control concept on the basis of the simplified flat system can be considered as adequate for vibration damping. An interesting investigation for the online identification of the parameters used for oscillation suppression would be the use of an adaptive control concept. This may be the topic of future work.

Taking a closer look at equation (16) implies the minimal required order of the trajectories for the flat outputs $\mathbf{z}$. On the one hand, cubic or even lower order trajectories will result in discontinuous input torques $\mathbf{Q}_M$ and as a consequence vibrations are induced. On the other hand, with an increase of the order, the minimum time to reach a desired point increases as well. Hence, when considering time-optimal motions, fourth-order trajectories are recommended for the given system.

An important fact to mention is that the calculation of the torques $\mathbf{Q}_A$ with the use of acceleration signals is not unproblematic for deriving the derivatives $\dot{\mathbf{Q}}_A$. A filter approximating the time differentiation of $\mathbf{Q}_A$ represents a sufficient trade-off. The optimal solutions for the given optimization problems are obtained using the MUSCOD-II toolkit. Therefore, a comparison to other optimization strategies would be interesting for verifying the optimality of the resulting solutions. Due to the fact that these problems are solved offline, the use of a model predictive control (MPC) strategy for utilizing the control for online time-optimal path-planning with finite horizons, may be considered. The MPC solves an optimization problem subject to given constraints in each sampling step. However, the highly nonlinear optimization formulation is thereby not unproblematic.

Conclusion

In this study, an approach to time-optimal trajectories for the use with theoretically any kind of elastic robot manipulator and experimentally for one specific flexible link system was shown. Therefore, an optimization problem for minimizing the trajectory duration for path constrained as well as point-to-point motions was formulated subject to physical constraints (velocity, jerk and drive torque). The bending of the beam must not be arbitrarily large for avoiding plastic deformation and enabling sufficient control of the induced oscillation. Hence, additional constraints for parts of the GFs (bending moments) and its derivatives were added to the optimization problem in order to avoid intense vibrations resulting from structural elasticities. By constraining only parts of the GFs and GFDs, a trade-off between not inducing oscillations, on the one hand, but also allowing fast trajectories, on the other hand, was achieved.

The proposed concept was verified using an elastic articulated robot with two flexible links. In order to obtain a sufficient dynamical model for the control concept as well as for constraint calculation, the equations of motion were obtained with the Projection Equation using a reduced lumped element model with spring-damper systems representing the elasticities. A two-degree-of-freedom control was used for trajectory tracking in combination with an active vibration damping. For trajectory generation, a fourth-order continuous path was optimized with respect to the dynamics of the simplified flat system. The TCP acceleration measurements, obtained when moving on the trajectories resulting from the optimization problem with and without consideration of the additional constraints, demonstrate the efficiency of this formulation. Furthermore, an analysis of the bending stresses showed that the maximal permissible bending stress is not violated when using these additional constraints. Future work will focus on implementing more complex models of the robot as this is one of the key issues when moving on constrained time-optimal trajectories.

Declaration of conflicting interests

The authors declare that there is no conflict of interest.

Funding

This study was funded by the Austrian Center of Competence in Mechatronics (ACCM).

References

1. Ozgoli S and Taghirad HD. A survey on theory control of flexible joint robots. *Asian J Control* 2006; 8(8): 1–15.
2. Li Y, Tong S and Li T. Fuzzy adaptive dynamic surface control for a single-link flexible-joint robot. *Nonlinear Dynam* 2012; 70(3): 2035–2048.
3. Li Y, Tong S and Li T. Adaptive fuzzy output feedback control for a single-link flexible robot manipulator driven DC motor via backstepping. *Nonlinear Anal: Real* 2013; 14(1): 483–494.
4. Schoenwaldt DA, Feddemat JT, Eisler GR, et al. Minimum-time trajectory control of a two-link flexible robotic manipulator. In: *Proceedings of the 1991 IEEE international conference on robotics and automation*, Sacramento, CA, 9–11 April 1991, pp.2114–2120. IEEE.
5. Kojima H and Kibe T. Optimal trajectory planning of a two-link flexible robot arm based on genetic algorithm for residual vibration reduction. In: *Proceedings of the 2001 IEEE/RSJ international conference on intelligent robots and systems*, Maui, HI, 29 October–3 November 2001, pp.2276–2281. IEEE.
6. Zhao H and Chen D. Optimal motion planning for flexible space robots. In: *Proceedings of the 1996 IEEE international conference on robotics and automation*, Minneapolis, MN, 22–28 April 1996, pp.393–398. IEEE.
7. Shin K and McKay N. A dynamic programming approach to trajectory planning of robotic manipulators. *IEEE T Automat Contr* 1986; 31(6): 491–500.
8. Pfeiffer F and Johanni R. A concept for manipulator trajectory planning. *IEEE J Robot Autom* 1987; 3(2): 115–123.
9. Shiller Z. Time-energy optimal control of articulated systems with geometric path constraints. In: *Proceedings of the 1994 IEEE international conference on robotics and automation*, vol. 4, San Diego, CA, 8–13 May 1994, pp.2680–2685. IEEE.
10. Constantinescu D and Croft EA. Smooth and time-optimal trajectory planning for industrial manipulators along specified paths. *J Robotic Syst* 2000; 17(5): 233–249.
11. Verscheure D, Demeulenaere B, Swevers J, et al. Time-energy optimal path tracking for robots: a numerically efficient optimization approach. In: *AMC '08. 10th IEEE international workshop on advanced motion control*, Trento, Italy, 26–28 March 2008, pp.727–732. IEEE.
12. Gattringer H, Riepl R and Neubauer M. Optimizing industrial robots for accurate high-speed applications. *J Ind Engineering* 2013; 2013: 1–12.
13. Bremer H. *Elastic multibody dynamics: a direct Ritz approach*. Heidelberg: Springer-Verlag, 2008.
14. Siciliano B and Khatib O. *Handbook of robotics*. Berlin-Heidelberg: Springer-Verlag, 2008.
15. Fliess M, Lévine J, Martin P, et al. Flatness and defect of non-linear systems: introductory theory and examples. *Int J Control* 1995; 61(6): 1327–1361.
16. Staufer P and Gattringer H. State estimation on flexible robots using accelerometers and angular rate sensors. *Mechatronics* 2012; 22(8): 1043–1049.
17. Leineweber DB. Efficient reduced SQP methods for the optimization of chemical processes described by large sparse DAE models. *Fortschritt-Berichte VDI Reihe* 1999; 3: 613.

Appendix

Notation

$\dot{a} = da/dt$	derivative with respect to time t
$a' = da/d\sigma$	derivative with respect to σ
$\mathbf{a}_1$	acceleration at the third joint
$\mathbf{a}_2$	acceleration at the tool center point

${}_R\mathbf{b}$	vector in frame R
$\mathbf{E}$	identity matrix
$\mathbf{F}$	Jacobian matrix
$\mathbf{f}^e$	impressed forces
$\mathbf{G}$	gyroscopic matrix with respect to minimal coordinates
$\overline{\mathbf{G}}$	gyroscopic matrix with respect to describing velocities
J	objective function
$\mathbf{J}$	moment of inertia
$\mathbf{K}$	stiffness matrix
$\mathbf{K}_{PM}, \mathbf{K}_{DM}, \mathbf{K}_{PQ}, \mathbf{K}_{DQ}$	controller gains
L	Lagrange term
$\mathbf{L}$	angular momentum
m	body mass
$\mathbf{M}$	mass matrix with respect to minimal coordinates
$\overline{\mathbf{M}}$	mass matrix with respect to describing velocities
$\mathbf{M}^e$	impressed moments
$\mathbf{p}$	linear momentum
$\mathbf{q}$	minimal coordinates
$\mathbf{Q}$	generalized force (GF) with respect to minimal coordinates
$\overline{\mathbf{Q}}^e$	GF with respect to describing velocities
$\mathbf{Q}_A$	GF due to joint torques/bending moments
$\mathbf{Q}_F$	GF due to friction
$\mathbf{Q}_{G,A}$	GF due to gravitational terms
$\mathbf{Q}_M$	GF due to motor torques
$\mathbf{r}$	tool center point position
$\mathbf{s}$	algebraic state vector
u	fourth derivative of σ
$\mathbf{u}$	fourth derivative of $\mathbf{q}_A$
$\mathbf{u}_{FB}$	feedback control
$\mathbf{u}_{FF}$	feedforward control
$\mathbf{u}_M$	MUSCOD-II control vector
$\mathbf{v}$	linear velocity
$\mathbf{V}_{el}$	elastic potential of the simplified system
W	section modulus
$\boldsymbol{\omega}$	angular velocity
$\boldsymbol{\omega}_{IR}$	angular velocity between frame I and R
$\mathbf{x}$	differential state vector
$\dot{\mathbf{y}}$	describing velocities
$\mathbf{z}$	flat output
$\mathbf{z}_d$	interpolated desired trajectory for the flat outputs
$\overline{\mathbf{z}}_d$	offline optimized desired trajectories for the flat outputs
$\boldsymbol{\eta}$	parameter vector
Φ	Mayer term
σ	scalar path coordinate
$\bar{\boldsymbol{\sigma}}$	path coordinate state vector
σ_b	occurring bending stress
σ_{bS}	maximum bending stress
σ_{max}	maximum permissible bending stress

Subscript

A	link coordinates
c	center of gravity
d	desired values
M	motor coordinates